

Red Clump Stars in the Sagittarius Tidal Streams

Kenneth Carrell^{1,2,3}, Ronald Wilhelm⁴ and YuQin Chen¹
 carrell@nao.cas.cn

ABSTRACT

We have probed a section ($l \sim 150$, $b \sim -60$) of the trailing tidal arm of the Sagittarius dwarf spheroidal galaxy by identifying a sample of Red Clump stream stars. Red Clump stars are not generally found in the halo field, but are found in significant numbers in both the Sagittarius galaxy and its tidal streams, making them excellent probes of stream characteristics. Our target sample was selected using photometric data from the Sloan Digital Sky Survey, Data Release 6, which was constrained in color to match the Sagittarius Red Clump stars. Spectroscopic observations of the target stars were conducted at Kitt Peak National Observatory using the WIYN¹ telescope. The resulting spectroscopic sample is magnitude limited and contains both main sequence disk stars and evolved Red Clump stars. We have developed a method to systematically separate these two stellar classes using kinematic information and a Bayesian approach for surface gravity determination. The resulting Red Clump sample allows us to determine an absolute stellar density of $\rho = 2.7 \pm 0.5$ RC stars kpc^{-3} at this location in the stream. Future measurements of stellar densities for a variety of populations and at various locations along the streams will lead to a much improved understanding of the original nature of the Sagittarius galaxy and the physical processes controlling its disruption and subsequent stream generation.

Subject headings: galaxy: halo — galaxies: interactions — stars: horizontal branch

1. Introduction

Since its discovery (Ibata et al. 1994), the Sagittarius dwarf spheroidal galaxy (Sgr) has served as an important probe for the understanding of the properties of our Galaxy. Unlike other previously identified Milky Way satellite galaxies, the Sgr is a relatively nearby galaxy with clear evidence of being tidally disrupted. Less than two years after its discovery the Sgr was found to have 'tidal tails' (Mateo et al. 1996) - stars which have been stripped from the main body of

the dwarf galaxy through its interaction with the Milky Way Galaxy. This led to the finding that the Sgr actually had an extended and prominent stream of stars that was ultimately traced over the entire sky (Majewski et al. 2003).

The core of the Sgr is located below the bulge of our Galaxy as seen from the location of the Sun. Its orbit has been found to be near polar and both leading and trailing streams of tidally stripped stars accompany the core. These streams trace out the full orbit of the Sgr and overlap each other at several locations (see, for example, the models of Johnston et al. (2005); Law et al. (2005); Fellhauer et al. (2006); Law & Majewski (2010)). It is currently not known how many orbits are represented in the streams, how long ago the stars were liberated from their host, the Sgr initial mass function (IMF), or the initial internal dynamics of the Sgr. All of these are important parameters that are needed to better constrain the Sgr orbital models. As these models become more

¹Key Laboratory of Optical Astronomy, National Astronomical Observatories, Chinese Academy of Sciences, Beijing 100012, China

²Physics Department, Texas Tech University, Lubbock, Texas 79409

³Visiting Astronomer, Kitt Peak National Observatory, which is operated by the Association of Universities for Research in Astronomy, Inc. (AURA) under cooperative agreement with the National Science Foundation

⁴Physics and Astronomy Department, University of Kentucky, Lexington, KY 40506

realistic much stronger constraints will be placed on the shape of the dark matter halo and the disruption processes that govern dwarf satellite accretion (see Gómez-Flechoso et al. (1999); Ibata et al. (2001); Helmi & White (2001); Helmi (2004a,b); Johnston et al. (2005); Fellhauer et al. (2006) and references therein).

In the last decade, much progress has been made in characterizing properties of the streams. The 2MASS and SDSS survey programs have provided a wealth of information on stream location and kinematics using various stellar populations. Specifically, giants (Bellazzini et al. 2003; Majewski et al. 2003) and turnoff stars (Newberg et al. 2002) were among the first to provide a wider view of the full system, while more recent work has been concentrated on the more evolved stars of the horizontal branch (HB), both on the blue (Yanny et al. 2009; Ruhland et al. 2011) and red (Correnti et al. 2010; Shi et al. 2012) ends. The HB provides some benefits not available in other stellar populations. The blue HB extends blueward of the thick-disk and halo main-sequence turnoff making sample selection much easier compared to stars redward of the turnoff. Furthermore, placement on the HB is dependent on the age and metal abundance of the star - those on the blue end are older (and, in general, more metal poor) with decreasing age (and, in general, increasing abundance) as a function of redder color. The HB terminates on the red end with a red clump of stars where the mechanism that drives the HB placement is no longer as effective in changing the color of the He-core burning star. This age/metallicity relation between the older, blue, metal-poor HB and the younger, metal-rich, RC can be exploited to probe changes in the contribution of stellar populations in the streams and Sgr proper.

In particular, a photometric study by Bellazzini et al. (2006) found a gradient in the ratio of old to young stars along the arms of the Sgr tidal streams. This study compared the ratio of BHB stars to RC stars in the core of the Sgr and in an area far from the core along one of the tidal streams. The authors found the BHB/RC ratio to be five times larger in the stream than in the core of the dwarf galaxy. This led Bellazzini et al. (2006) to conclude that a steep, radial, age/metallicity gradient must have been present in the progenitor Sgr prior to the

tidal stripping events that produced the stream. This result was based solely on star counts from photometric data where contamination from various sources (galaxies in the BHB colors and foreground disk stars in the RC colors) were difficult to eliminate.

This current paper is part of a program to observe RC stars spectroscopically and to confirm their stream membership through kinematics and surface gravity determinations. This method greatly reduces the effects of background contamination. A clean sample of RC stream members is used to determine the stellar density of stars at one point along the Sgr stream. This program, coupled with stellar densities from other populations, ultimately holds the potential for the reconstruction of the Sgr IMF, initial stellar distribution, and clues to the internal dynamics of the progenitor Sgr.

In section 2 of this paper we will discuss the sample selection criteria and the observations and reductions of our spectroscopic data. Section 3 describes the analysis procedure used to provide a clean RC sample. In section 4 we present the results found using this stellar sample and follow it up in section 5 with a discussion of these results.

2. Data

2.1. The Sample

Our candidate stars were selected using the Sloan Digital Sky Survey (SDSS) online database². Using previous measurements (Majewski et al. 2003, 2004) and simulated models (Law et al. 2005; Fellhauer et al. 2006; Law & Majewski 2010) of the Sgr tidal tails, a dynamically cold and kinematically distinct region of the stream was chosen for study. The kinematic signature will aid in eliminating contaminants in our color selection (disk dwarfs and halo giants). We chose to observe a region of the trailing arm at (l,b) of approximately $(150^\circ, -60^\circ)$. This region had the advantages of being previously studied by other investigators and a known stream distance (less than 40 kpc) which fell within the limiting magnitude ($g \sim 19$) for our current project. In addition, the models of Law et al. (2005) predict that the more dispersed leading arm overlaps in distance at this location.

² <http://www.sdss.org>

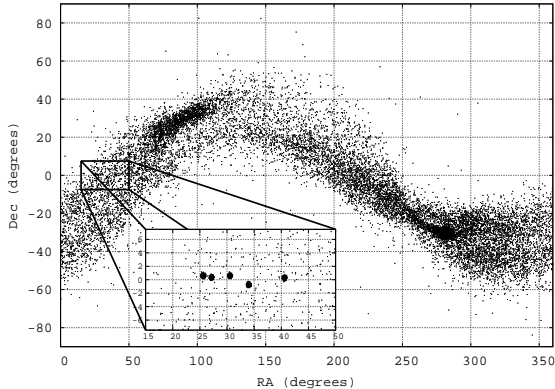


Fig. 1.— Equatorial coordinates for the triaxial halo model of Law & Majewski (2010) and the fields observed in this research. The filled circles in the inset correspond to observed fields. The core of the Sgr dwarf galaxy is the clump of stars located at $(RA, Dec) \sim (285^\circ, -30^\circ)$.

This afforded us the possibility of detecting the leading arm within the same dataset.

The expected stream distances at this location are ~ 30 kpc and the streams should be dynamically cold with predicted velocities for the leading (trailing) arm of roughly $+(-)150$ km s^{-1} . These velocities are uniquely different from the larger number of contaminating disk stars which have velocities of nearly 0 km s^{-1} in this direction and the halo which has an average velocity slightly less than -100 km s^{-1} in this direction and has a large velocity dispersion. This insured that stream identification could be made, in part, from the kinematics of the RC stars. Table 1 shows relevant values for our selected fields and Figure 1 shows our field positions in right ascension and declination overlaid on the triaxial halo model of Law & Majewski (2010).

To choose our candidate stars, color and magnitude cuts were determined that would encompass the Sgr RC stars while minimizing contamination from stars in the disk of our Galaxy. To establish the color boundaries for the RC in the Sgr galaxy we used the extinction corrected $V - I$ photometry data of Layden & Sarajedini (2000). We then transformed these color boundaries to the SDSS photometric system using photometric transformation equations by Robert Lupton on

Table 1: Field Locations

Field	RA (degrees)	Dec (degrees)	l (degrees)	b (degrees)
f02	27.15	+0.383	151.8	-59.25
f05	25.63	+0.633	148.9	-59.64
f09	30.55	+0.633	157.3	-57.44
f11	34.02	-0.717	164.0	-56.68
f18	40.60	+0.317	171.7	-51.74

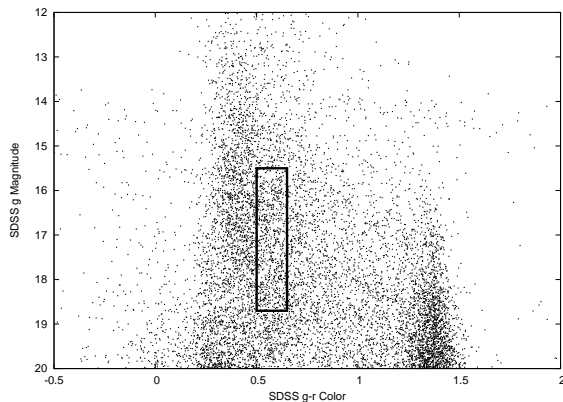


Fig. 2.— A representative color-magnitude diagram of stars in our selected area of the sky. The box represents the selection criteria used to select the RC program stars of $0.5 < (g - r)_o < 0.65$ and $15.5 < g_o < 18.7$.

the SDSS website³. The magnitude range was influenced by the expected distances of stream stars (30 kpc corresponds to a g magnitude of slightly fainter than 18 assuming an absolute magnitude of $g_{abs} \sim 1.0$), telescope aperture, and the reliable range of the SDSS photometry. Our final adopted selection criteria were $0.5 < (g - r)_o < 0.65$ and $15.5 < g_o < 18.7$. Figure 2 is a representative g_o versus $(g - r)_o$ CMD for candidate stars in one of our fields with the selection box overlaid. The range in magnitude corresponds to a distance range of roughly 8 to 35 kpc (assuming an absolute magnitude of $g_{abs} \sim 1.0$). This magnitude range insured the inclusion of all RC stars in the primary trailing arm and also allowed for the inclusion of other, nearer portions of the stream that are suggested from the stream models.

³ <http://www.sdss.org/dr6/algorithms/sdssUBVRITransform.html>

While the chosen color and magnitude range encompasses the candidate RC stars, it also allows for the inclusion of a significantly large number of contaminating main-sequence stars from the Galactic disk. In addition to the disk stars there is also a relatively small number of K giants that are expected from both the halo field and the Sgr stream. To minimize the contamination from both the disk and halo field we used a combination of kinematics and computed surface gravities. The kinematic signature from the dynamically cold stream is easily distinguished from both the disk and halo populations. Furthermore, the surface gravity for the RC stars is significantly lower than the main-sequence stars in the disk. By combining both the kinematic information and the stellar surface gravity determinations we are able to get a clean sample of stream giant stars.

2.2. The Observations

The spectroscopic observations were taken at the WIYN telescope at KPNO using the Hydra instrument. Observations were carried out in August 2007. Hydra has 83 active blue fibers that have a diameter of 3.1 arc-seconds on the sky and are positioned within the 1° diameter field of view. The Simmons Camera with no filter and a 600 lines per mm grating with a central wavelength of 5500 Å was used. This gave a resolution of approximately 4.6 Å and a dispersion of just over 1 Å per pixel. Our detector setup provided us with a wavelength coverage of roughly 4000-5500 Å. The density of candidates and the positioning constraints of the instrument allowed on average 42 objects to be simultaneously observed in each field.

For each program field, four, 30 minute integrations were obtained, cleaned of cosmic-ray events and co-added, for a total integration time of two hours per field. This exposure time resulted in data with a typical SNR of ~ 45 at a g_o magnitude of 16.5 and ~ 20 at a g_o magnitude of 18.

The reduction of all images was performed using the IRAF software package⁴. Bias level subtraction, flat-field division using dome flats, sky subtraction, spectral extraction, and wavelength calibrations from a CuAr lamp were all performed using the *dohydra* routine in IRAF.

⁴<http://iraf.noao.edu>

3. Analysis

In an effort to extract meaningful information from the spectral data obtained as described in section 2, an analysis software framework was developed by the authors. The ability to separate the RC stream stars from main sequence disk stars hinged on the ability to determine the kinematics of our sample as well as reliable stellar parameters. Of particular interest is the ability to quantify surface gravity since this parameter is a key discriminator for the RC sample.

3.1. The Procedure

Our procedure uses a grid of synthetic spectra to compare to our observed data. The synthetic stellar spectra were generated using the SPECTRUM program⁵ with ATLAS9 model atmospheres⁶ as input. These grids were generated to encompass the entire parameter space likely to be observed in the program stars. The grid size for the effective temperature was 4000 to 6000 K with a step size of 250 K. For surface gravity a step size of 0.5 dex was used over a range of 0.5 to 5.0 dex. The metallicity range was -2.5 to +0.5 dex in increments of 0.5 dex.

A primary concern we had with the synthetic data (as well as the scientific data) was how the normalization would be carried out. While SPECTRUM allows for the synthetic spectra to be output in a normalized form, this true normalization can be quite different from the normalized, pseudo-continuum found for the science data by fitting the non-flux calibrated spectra. Direct comparison between the two normalizations leaves open the possibility that systematic errors could be introduced in the form of incorrect line strengths because of incorrect continuum placement. To avoid this possible problem, the synthetic spectra were output with absolute flux values and both these and the observed spectra were normalized by fitting the continuum with a third order polynomial.

A table of the wavelength ranges used to determine each parameter can be found in Table 2. We are using strictly the H_β line as a tem-

⁵Developed by Richard Gray, <http://www.phys.appstate.edu/spectrum/spectrum.html>

⁶From Robert Kurucz, <http://kurucz.harvard.edu>

Table 2: Wavelength Regions for Parameter Determinations

Wavelength Range (Å)	Parameter
4840 - 4880	T_{eff}
5000 - 5250	$\log g$
4360 - 4400	[Fe/H]
4630 - 4680	[Fe/H]
4900 - 4930	[Fe/H]
4970 - 4990	[Fe/H]
5030 - 5050	[Fe/H]
5220 - 5290	[Fe/H]
5435 - 5465	[Fe/H]

perature indicator and the wavelength region that includes the magnesium b lines and magnesium hydride molecule as a surface gravity indicator. Other areas were investigated for both parameters but nothing was found to improve the results from these single ranges. Our abundance information is spread over the entire observed wavelength range but excludes the previously mentioned areas used for other parameters. In Figures 3, 4, and 5 are some example spectra for the wavelength ranges used to determine the stellar parameters. The stars in these plots have a signal to noise in the middle of our observed range.

The full spectrum was used in determining the velocities of the program stars by employing a method of steepest descent to find a minimum of the sum of the squares of the differences between the data and synthetic spectra. Once a radial velocity was found, it was transformed into different rest frames for easier comparison with both previous observations and different models. In particular, the values given by Schönrich et al. (2010) were adopted to correct to the local standard of rest (v_{LSR}), and a solar circular velocity of 225 km s^{-1} was used to determine velocities in the Galactic rest frame (v_{GSR}).

The method of extracting all the relevant information for a given star began with determining its radial velocity. After finding this initial velocity, an initial set of stellar parameters were determined. In order to accomplish this task, a Bayesian approach was implemented. Specifically, we used a Bayesian posterior distribution defined

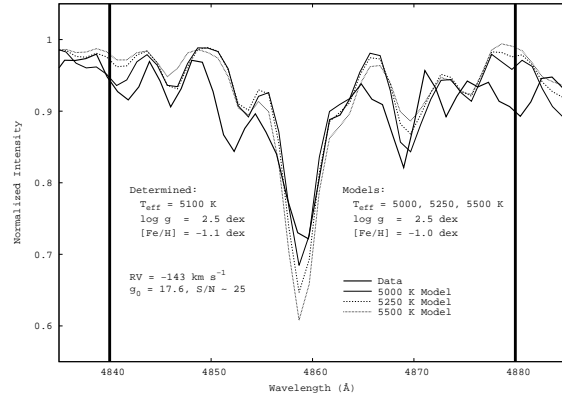


Fig. 3.— Normalized example spectrum of an observed star showing the wavelength range used to determine the effective temperature (marked with vertical lines). Spectroscopic data is shown with a thick solid line. The synthetic data has been shifted to match the determined radial velocity of the star. The major feature in this range is the H_{β} line.

as

$$P_A \propto L * P_B$$

where P_A and P_B are the posterior and prior probabilities respectively and L is the likelihood which we define as

$$L = e^{-\chi^2/2},$$

$$\chi^2 = \sum_i \left(\frac{f_{o,i} - f_{s,i}}{\sigma_i} \right)^2$$

where the sum is over the observed data points in the wavelength range of interest, the subscript o denotes an observed value, the subscript s denotes the synthetic value at the same wavelength and the flux, f , has been normalized. The synthetic flux values are evaluated at the observed wavelength value using a cubic spline interpolation. The variable σ_i is the normalized noise estimate of the data determined from the non-normalized flux F at each data point and defined as

$$\sigma_i = \sqrt{\frac{2}{F_{o,i} * GAIN}}$$

which is derived from the equation given by Massey & Jacoby (1992) for 'ugly data.'

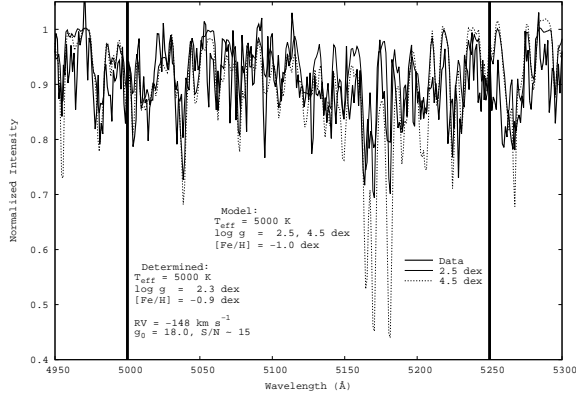


Fig. 4.— Normalized example spectrum of an observed star showing the wavelength range used to determine the surface gravity (marked with vertical lines). Spectroscopic data is shown with a thick solid line. The overlaid synthetic spectra have been shifted to match the determined radial velocity of the star. The magnesium b lines are the dominant feature in this wavelength range.

We sequentially determine the stellar parameters and use each new result as a prior distribution for the next. Since we require some initial prior probability to get this method started, we use the precise photometry available from the SDSS database along with the effective temperature’s dependence on $(g - r)_0$ color given by Fukugita et al. (2011) as a prior probability distribution for our effective temperature determination. Specifically, we use a Gaussian centered on the temperature given by their equation using the $(g - r)_0$ color of the star with a width of 250 K (which is the spacing of our synthetic grid). In Fukugita et al. (2011) they quote an rms scatter of 93 K, but we only want this prior to guide our spectroscopic temperature determination so we use the wider width of the grid spacing so as not to force our result to the photometrically determined value. We then compute the likelihood at each synthetic grid point using the H_β region of the spectrum. Combining the likelihoods and prior probability distribution gives us the posterior probability distribution for the effective temperature. We next determine the posterior probability distribution for the metallicity of the star using the effective temperature’s posterior probability as the prior probability and the likelihoods

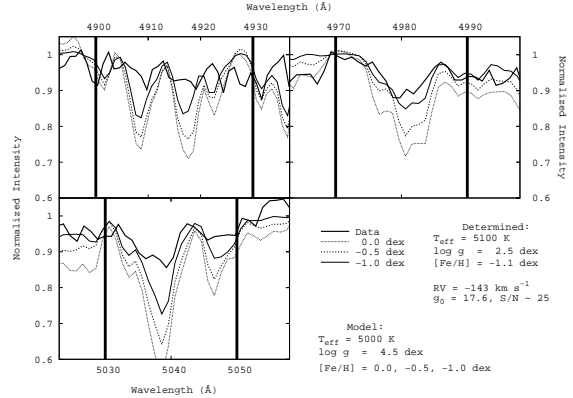


Fig. 5.— Normalized example spectrum of an observed star showing three of the wavelength ranges used to determine the metallicity (marked with vertical lines). Spectroscopic data is shown with a thick solid line. The overlaid synthetic spectra have been shifted to match the determined radial velocity of the star. These wavelength ranges include primarily Fe lines.

calculated based on the wavelength ranges mentioned above and shown in Table 2. Finally, we use both the effective temperature and metallicity posterior probabilities as the prior probability for the surface gravity determination and calculate the likelihoods in the same manner as the other two parameters. The actual parameters (and their associated errors) are determined from the normalized posterior probability distributions. The most likely values (i.e. the parameters) are just the weighted averages of each distribution and the errors are the weighted standard deviations.

There are numerous ways that one can use the Bayesian approach to determine the stellar parameters in a similar manner. We have chosen the approach described above because the parameter we are most interested in is the surface gravity. This parameter is difficult to determine and the added information from the other two parameters in the form of prior probabilities improves our results. This could result in the other two parameters being less certain, but as we show in the next section, the overall properties of the RC sample are consistent with the expectations of these types of stars in the Sgr tidal debris.

After finding an initial set of stellar parameters, we perform another round of radial velocity and

parameter determinations. While we don't expect the values to change significantly, this second iteration of finding both the radial velocity and stellar parameters insures that we have the best possible values. In particular, we want to use the closest matching grid points to determine the radial velocity and we want the best radial velocity to determine the final parameters. Therefore, we adopt the second iteration values as our parameters although there is little change between the two sets of values.

3.2. Calibration and Validation

In order to test the validity of our parameter determinations, we used the results of the stars in our observed sample that were also spectroscopically observed by the SDSS. This is a rigorous test of our method and software since we are able to run our routine on the spectra obtained both by the SDSS and on WIYN. A comparison of the parameters determined with our routine using SDSS spectra to those determined by the SEGUE stellar parameter pipeline (SSPP) is a direct test of the accuracy of our parameter estimation method. Furthermore, a comparison of parameters from the WIYN data not only our depends on our routine, but the different data sets as well. There were approximately 70 stars in common and we found good agreement between all three sets of parameters with no large offsets or systematic trends. When running our software on SDSS spectra and comparing the results with those of the SSPP, we have mean absolute differences of 110 K, 0.2 dex, 0.1 dex, and 7 km s⁻¹ in effective temperature, surface gravity, metallicity, and radial velocity, respectively. The standard deviations of the differences in the effective temperature, surface gravity, metallicity, and radial velocity are 75 K, 0.2 dex, 0.2 dex, and 3 km s⁻¹, respectively. When comparing the parameters from our WIYN spectra to those of the SSPP we find mean absolute differences of 25 K, 0.05 dex, 0.2 dex, and 8 km s⁻¹ and standard deviations of 100 K, 0.4 dex, 0.7 dex, and 9 km s⁻¹ for the effective temperature, surface gravity, metallicity, and radial velocity, respectively.

Since we are most interested in the surface gravities because of the ability to separate dwarf stars from giant stars, a comparison plot and residual histograms for this parameter are given in Figures

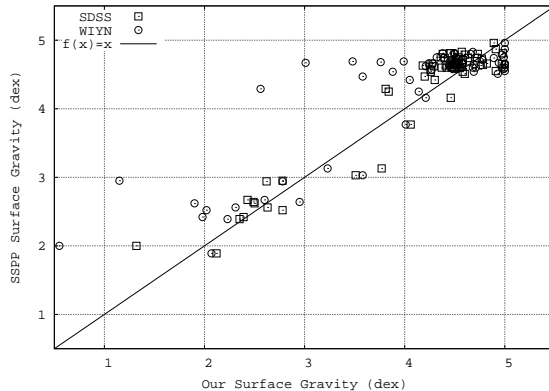


Fig. 6.— A comparison of the surface gravity values determined from SDSS (squares) and WIYN (circles) spectra using our stellar parameter determination routine as described in the text. Our values are along the horizontal axis and the SEGUE stellar pipeline values are along the vertical axis.

6 and 7, respectively, to better show the quality of our parameter determination. The Gaussian fit to the WIYN data in Figure 7 finds $\sigma = 0.4$ dex, which we take as a measure of error for our entire sample. On a star by star basis the errors on the surface gravities are slightly higher (on average 0.5 dex) but not significantly so. Our routine returns surface gravities for the WIYN spectra which are not quite as precise as values from the SEGUE stellar pipeline, but this is expected since we use spectra with relatively low S/N.

The radial velocities from the WIYN spectra have a slight offset (~ 8 km s⁻¹) with respect to the SDSS pipeline values. We use this offset to calibrate our radial velocities. In Figures 8 and 9 one can see the agreement between our results and the SEGUE stellar pipeline. In these plots, the values from the WIYN spectra have been calibrated to account for the small offset while the values from the SDSS spectra have not. The published pipeline velocities also have a small offset applied (see section 2.2 from Lee et al. (2008) and the spectroscopic caveats webpage⁷ for DR8), which is similar to the difference we find between the WIYN stars and the stellar pipeline values. Further, there is no obvious systematic across a velocity range spanning roughly 500 km s⁻¹ so

⁷<http://www.sdss3.org/dr8/spectro/caveats.php>

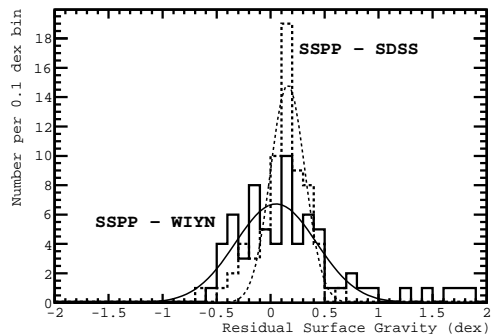


Fig. 7.— Residual histograms of surface gravities determined from SDSS (dashed) and WIYN (solid) spectra using our stellar parameter determination routine subtracted from SEGUE stellar pipeline values. The Gaussian fits that are overlaid have widths of 0.2 and 0.4 dex for the SDSS and WIYN data, respectively.

calibrating our velocities using this small offset should not affect our results significantly.

As a consistency check, we look at the properties of our selected RC sample and how it compares to previous results. For our RC sample we find an average T_{eff} of 5240 K with a standard deviation of 220 K. The empirical calibration of Alonso et al. (1999) (Equation 6 in their Table 2) for F-K giants gives a temperature of 5480 K with a standard deviation of 125 K in the middle of our $(V - I)_o$ color range ($(V - I)_o = 0.9175$). Using the color- T_{eff} relation of McWilliam (1990) (Table 6) we find a temperature of 5580 K with an uncertainty of 80 K using the middle of our color range. Our T_{eff} values agree better with SSPP values, but this comparison suggests that our temperatures may be systematically too cool by up to 300 K. Our average metallicity for the RC stars is -0.5 dex, which is in agreement with previous metallicity estimates of the Sgr dwarf galaxy system (see, e.g., Chou et al. (2007) and their discussion in section 2 of the paper). The standard deviation on the mean of our metallicity is 0.7 dex which is primarily due to the low resolution and S/N of our spectra.

In summary, we have implemented a statistically sound and robust method for determining relevant properties of stars using a Bayesian ap-

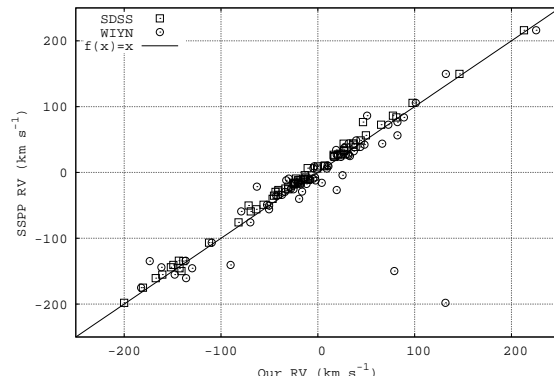


Fig. 8.— A comparison of the radial velocities determined from SDSS (squares) and WIYN (circles) spectra using our stellar parameter determination routine as described in the text. Our values are along the horizontal axis and the SEGUE stellar pipeline values are along the vertical axis.

proach. This method provides results that are in good agreement with results from the SEGUE stellar pipeline for stars observed both on WIYN and by the SDSS. We are therefore confident that we can use the results of this routine to separate populations of stars based on their stellar parameters and kinematics.

4. Results

As was described in section 2.1, our selection criteria allowed for the inclusion of quite a significant background, namely the disk of our Galaxy. Since we observed stars spectroscopically, however, we were able to take advantage of the fact that the stream and disk stars are in different stages of the stellar life cycle. This coupled with the velocity information provides discrimination between the stream and disk stars. We will first describe the procedure used to select the stream stars from our full sample and will follow that with the results these stars provide us.

4.1. Separating the Sample

Figure 10 shows a histogram of heliocentric velocities for all the stars observed in our 5 WIYN fields that have g_o magnitudes fainter than 16.5 as well as stars obtained from the Besançon stel-

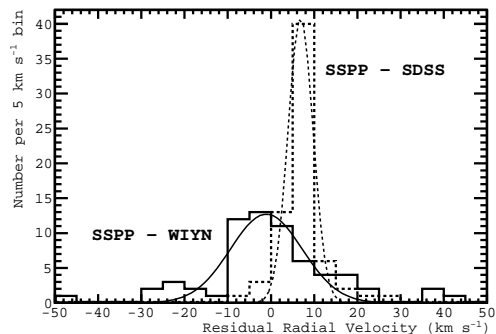


Fig. 9.— Residual histograms of radial velocities determined from SDSS (dashed) and WIYN (solid) spectra using our stellar parameter determination routine subtracted from SEGUE stellar pipeline values. The Gaussian fits that are overlaid have widths of 3 and 8 km s⁻¹ for the SDSS and WIYN data, respectively. Note that the WIYN data has been calibrated by accounting for a small offset while the SDSS data has not.

lar population synthesis model of the Galaxy⁸ (Robin et al. 2003) using the same selection criteria as the observations. In this histogram one clearly sees disk velocities in our WIYN sample match those from the model (~ 0 km s⁻¹) and are the dominant component. It is important, however, to note that even in the full sample there is a noticeable kinematic signature of stream stars in the distribution. In the plot of heliocentric velocities as a function of surface gravity for our full sample of stars shown in Figure 11, one sees exactly what is expected if the dynamically cold component of the kinematic distribution is due to RC type stars in the Sgr streams: a large number of stars with low velocities (~ 0 km s⁻¹) and high surface gravities ($\gtrsim 4$ dex in $\log g$) as well as a population with lower surface gravities ($\lesssim 3.0$ dex) and very different velocities (~ -150 km s⁻¹). The former group is undoubtedly the disk stars in our sample and the latter is the RC stars in the tidal streams of the Sgr. In Figure 11 the sample has been separated with a cut of $\log g < 3.0$ dex where stars that agree with this bound including errors we label as possible stream stars and those not satisfying it are labeled as disk dwarfs. As was men-

⁸<http://model.obs-besancon.fr>

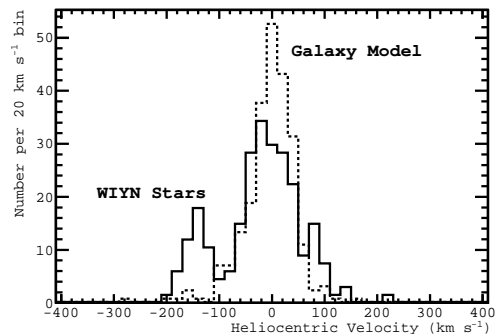


Fig. 10.— Histogram of the heliocentric velocities of all stars observed in our 5 WIYN fields (solid) and those from the Besançon model (dashed). The contamination from the disk in the WIYN data is the large peak with a mean of ~ 0 km s⁻¹ that overlaps with the expected disk velocities from the model. Stream stars are clearly visible as the smaller peak with velocities of ~ -150 km s⁻¹.

tioned in section 3.2, the comparison with stars having both SDSS and WIYN spectra gives us a typical surface gravity error estimate of 0.4 dex and our individual error estimates for the WIYN stars give us a typical error of 0.5 dex. One can see in Figure 11 that this is indeed the case by examining the stars with surface gravities between 3.0 and 3.5 dex to see which have been included in our low surface gravity sample. Representative errors for both our surface gravities and our radial velocities are shown for reference in the upper left corner of the figure.

Before determining a density, we must determine the quality of our sample of RC stars with regard to all possible contaminants. This portion of the H-R diagram contains several stellar types such as older stars including the metal poor K giants, the metal weak RHB stars and of course, potential contamination from the large population of main sequence stars. We have shown that by removing the higher surface gravity stars from the sample the contamination of disk type stars is minimal. To determine the level of contamination from the halo we use the Besançon model to generate a sample of Galactic stars (including all components) from our observed area of the sky and apply the surface gravity cut to eliminate disk

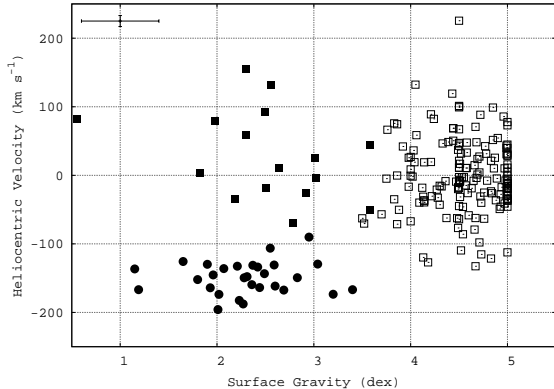


Fig. 11.— Heliocentric velocity versus surface gravity for our full sample of observed stars. The filled symbols are stars that satisfy the condition $\log g < 3.0$ dex within errors. Circles are stars which are also within 3σ of the fitted Gaussian mean for the group of stars with velocities of ~ -150 km s $^{-1}$. Representative errors for both parameters are given in the upper left corner.

dwarfs. Histograms of heliocentric velocities for our data and the Besançon model data which satisfy the surface gravity selection cut can be found in Figure 12. The Besançon model halo stars, chosen from our $\log g$ cut, are quite different from the RC sample. The RC stars show a large peak with kinematics that are consistent with other publications of the trailing arm of the Sgr in this location (as shown below). Other than the primary stream peak, our sample only shows one very small group of stars centered under the disk velocity distribution. We expect that this small peak may be a very small number of contaminating disk and/or halo stars. To estimate the level of contamination from misidentified dwarf stars we look at the number of outliers in Figure 6. There are five stars that have SSPP surface gravities greater than 4.0 dex and are different from our surface gravities by 0.75 dex (which would put them within or near our surface gravity criteria). Scaling this number by the fraction of observed stars in our sample (169 for stars fainter than $g_o = 16.5$) to comparison stars (67) gives us approximately a dozen (12.6) stars, which is exactly how many stars we find outside the narrow peak corresponding to the Sgr stream velocity in Figure 12.

We note that there could also be a small num-

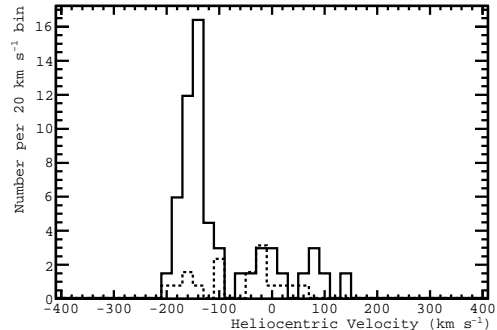


Fig. 12.— Histograms of heliocentric velocity for our observed data (solid) and the Besançon model data (dashed) which satisfy the surface gravity cut described in the text and have g_o magnitudes fainter than 16.5.

ber of contaminating K giants in the tidal streams (i.e. actual Sgr stream stars and not halo stars) as well since the Sgr has an older and more metal poor population as seen in the CMD of Layden & Sarajedini (2000). The number of metal poor giants is relatively low, however, and especially so when focusing on a small magnitude range as we do in the following. Further, even though Bellazzini et al. (2006) find that the relative number of BHB stars (older population) are enhanced in the tidal streams, they find that BHB stars still only account for 15% of the total BHB and RC stars. When comparing the number of K giants within our color-magnitude selection criteria to BHB stars in the Sgr proper (using the counts of BHB and metal poor giants from Layden & Sarajedini (2000)), the expected number of K giants is a factor of two less than the number of BHB stars. Assuming the 15% BHB contribution from Bellazzini et al. (2006), the percentage of K giants in the stream should be at most $\sim 7.5\%$ of the RC sample.

To be sure that we are indeed seeing the trailing arm of the Sgr tidal streams, we compare our results with those of previous works. Figure 13 shows that the GSR velocities for stars with low surface gravities match very well with those from Yanny et al. (2009) and Majewski et al. (2004).

In Figure 14 we show how the heliocentric velocities vary with g_o magnitude. The same surface

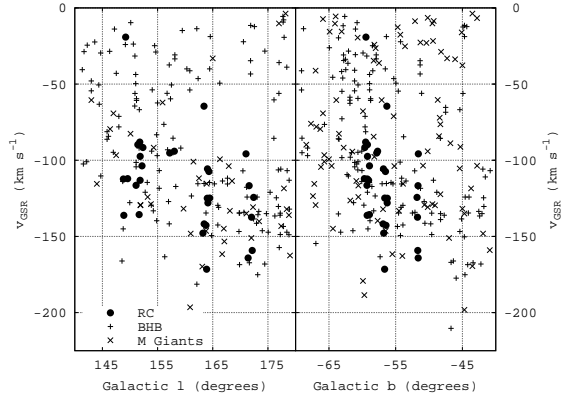


Fig. 13.— GSR velocities of our RC sample (filled circles), the BHB sample (+) from Yanny et al. (2009) and the M giant sample (x) from Majewski et al. (2004) as a function of Galactic l (left) and b (right).

gravity cut has been applied in this plot and one sees that not only do the low gravity stars have similar velocities, they also have similar magnitudes. This point is important because the RC is a part of the HB and we expect that their absolute magnitudes should all be roughly the same. Therefore, using g_o as a proxy for the distance, our low surface gravity sample has a large group of stars with similar distances according to Figure 14. Also in the plot one notices several vertical lines which correspond to possible magnitude limits which will be used in the density calculations. These limits are at g_o magnitudes of 16.5, 17.4, 17.85 and 18.7 (which is the magnitude limit of our observations). In Figure 15 we see that our RC distances are similar to the previous results of Yanny et al. (2009) and Majewski et al. (2004) by adopting an absolute magnitude of $g_{abs} = 1.0$.

We find no evidence of the leading arm in this area of the streams and at these distances. The leading arm would have velocities of $\sim +150 \text{ km s}^{-1}$ according to the models and we see no obvious kinematic feature other than that matching the trailing arm. The leading arm in our observed area would be much farther along the orbit from the Sgr compared to the trailing arm, which means the stars would have been pulled from the galaxy much earlier in the interaction history with our Galaxy. This suggests, qualitatively, that the RC stars were not loosely bound to the Sgr during

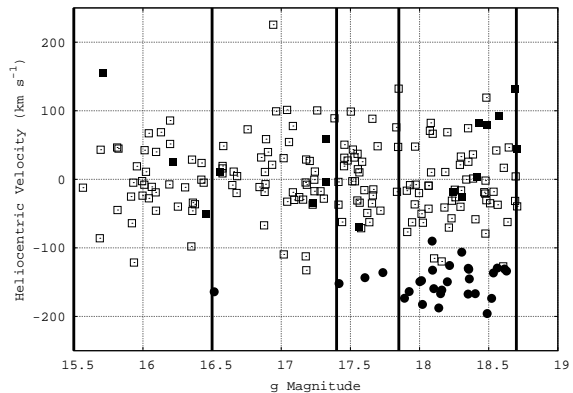


Fig. 14.— Heliocentric velocity versus g_o magnitude for our full sample of observed stars. The filled symbols are stars that satisfy the condition $\log g < 3.0$ dex within errors. Circles are stars which are also within 3σ of the fitted Gaussian mean for the group of stars with velocities of $\sim -150 \text{ km s}^{-1}$. The vertical lines correspond to g_o magnitudes of 16.5, 17.4, 17.85 and 18.7.

that time.

Since our color selection isolates the region of the RC seen in the Sgr proper and we see stars with low gravities that have similar velocities (which are different from any Galactic component in the same direction) and similar magnitudes, we are confident that these stars are RC stars in the trailing arm of the tidal streams of the Sgr.

4.2. Density of RC Stream Stars

The number of stars observed with different g_o magnitude limits can be found in Table 3. As can be seen in the table, our observations probed up to 76% of the stars with clean SDSS DR6 photometry in this region of the sky with these color and magnitude cuts. The candidate selection and placement of stars on fibers of the instrument is more or less completely random⁹ so we assume our sample has no selection bias. A small amount of metallicity bias is possible since the color of the RC is affected by metal abundance. However, the width of the color selection window is such that we

⁹Priority can be put on certain stars but that does not guarantee their placement. It only sets an order the software uses to attempt to configure the field and makes little practical difference.

Table 3: Star Counts

Bright Limit	Observed Fraction	RC Stars		Model Stars	
		Scaled	Integral	Scaled	Integral
$g_o > 16.5$	169/252	41.8	41.5	5.5	4.9
$g_o > 17.4$	122/169	37.4	37.0	3.9	3.7
$g_o > 17.85$	87/114	31.4	32.3	0.8	0.8*

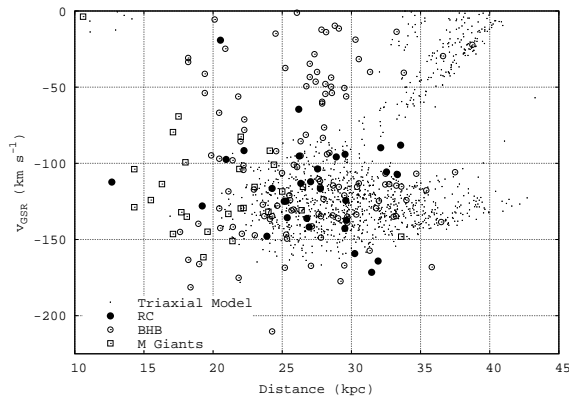


Fig. 15.— GSR velocity versus distance for our RC stars (filled circles), the BHB sample (open circles) from Yanny et al. (2009), the M giant sample (open squares) from Majewski et al. (2004) and the triaxial model (points) of Law & Majewski (2010).

expect this bias to be inconsequential. This allows us to scale our observed results up to what would be expected if we had observed every possible star in this area of the sky.

With this information we are now ready to compute the density of RC stars in the trailing arm of the Sgr. Each circular WIYN field has a diameter of 1° and we must multiply by the 5 fields to get a total area of our observations. The depth of the observation was established by using an estimate of the appropriate absolute g magnitude. In Yanny et al. (2009) an absolute magnitude of $g_{abs} = 0.7$ was used for BHB stars which could also be adopted here. However, the RC has a higher abundance than the BHB and this will affect the absolute magnitude of these HB stars. We determine the absolute magnitude for the Sgr RC using the measurements of Layden & Sarajedini (2000). In their work they give the location of the RC in their CMD and measure a distance

modulus to the Sgr using RR Lyrae stars. Using this information and their reddening and extinction values then converting to SDSS magnitudes we find $M_g = 1.0 \pm 0.1$ for the absolute magnitude of the RC. One could also use the age and metallicity for the intermediate age stars given by Layden & Sarajedini (2000) to find the absolute magnitude based on the local RC absolute magnitude and a correction from globular clusters (such as in Percival & Salaris (2003)). The same magnitude is found using this method as the above within errors. We calculate the density using both the absolute magnitude derived from the measurements of Layden & Sarajedini (2000) and the one adopted by Yanny et al. (2009) for the BHB in the following, but note that our derived value more closely matches the properties of the RC. In Figure 16 we plot the mean and standard deviation of the GSR velocities and distances for our RC sample, the Yanny et al. (2009) BHB sample, the Majewski et al. (2004) M giant sample and the triaxial halo model of Law & Majewski (2010) in our observed area. One sees that using an absolute magnitude of $M_g = 1.0$ we get very good agreement with both the BHB and model stars. The M giants look to be systematically closer but this is likely due to the limiting magnitude of their sample. The volume encompassing our sample was computed by determining the volume of a cone truncated at the bright end of our sample.

We determine the total number of stream stars using two methods. The first method we use is simply counting the stars which satisfy our surface gravity criterion ($\log g < 3.0$ dex within errors) and have heliocentric velocities that agree with the models and previous measurements ($-200 \text{ km s}^{-1} < v < -100 \text{ km s}^{-1}$). The other method we use is to fit the kinematic peak of the stars satisfying the surface gravity criterion with a Gaussian function and find the integral of this function out to 3σ from the mean. The fitted mean

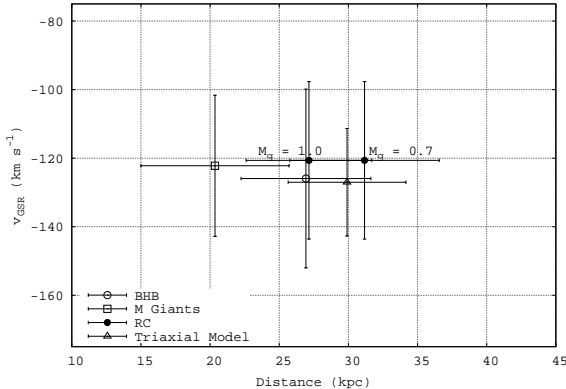


Fig. 16.— Mean (point) and standard deviation (error bar) of the GSR velocities and distances for the BHB sample (open circle) from Yanny et al. (2009), the M giant sample (open square) from Majewski et al. (2004), the triaxial model (open triangle) of Law & Majewski (2010) and our RC stars (filled circles) using two absolute magnitudes. All samples are constrained to our observed area and velocities of $-225 < v_{GSR} < -75$.

Table 4: Fitted mean and dispersion of heliocentric velocity of RC Sgr stream stars.

Bright Limit	μ (km s ⁻¹)	σ (km s ⁻¹)
$g_o > 16.5$	-148	21
$g_o > 17.4$	-147	21
$g_o > 17.85$	-148	24

and σ values for our sample of RC stream stars for different magnitude limits can be found in Table 4. Both methods should (and do) give similar results, but the latter is not affected by the arbitrary choice of defining velocities for the stream stars, rather it is determined directly. Contamination from halo K giants is determined in a similar manner (both with fits and from raw counts) from the Besançon model data. The RC counts are then scaled by our observed fraction and the model stars are scaled to our actual observed area to get the total number of RC and model (halo) stars in this area of the sky. To find the actual number of expected RC stars in our sample we subtract the number of model (halo) stars from our counts of RC candidates. We use Poisson noise as an error estimate for our star counts on both

the model (halo) and RC candidate samples. A table showing the star counts with different limiting magnitudes can be found in Table 3.

It is evident from the table that both the number of RC stars and the number of model halo stars decreases as the magnitude limit is decreased. However, the halo stars decrease to approximately a single star in the smallest magnitude range. In fact, there were so few stars in the model sample that a Gaussian fit could not be reliably determined, and therefore we use the raw count for the estimate of the fitted value in the faintest magnitude range. Furthermore, in Figure 14 it is obvious that most of our candidate RC stars are in the faintest magnitude range and those with similar velocities to the stream at brighter magnitudes are consistent with the number of halo giant stars expected in the sample. These two facts leads us to only consider stars with magnitudes of $17.85 < g_o < 18.7$ for our best density estimate. This density of $\rho = 2.7 \pm 0.5$ RC stars kpc⁻³ as well as the densities of the other magnitude ranges are summarized in Table 5. The final densities for each magnitude range are determined by taking the RC star counts (which have been scaled by our observed fraction and have the scaled number of model stars subtracted out) and dividing by the volume for the given absolute magnitude value. Errors on the counts are described above and are used to determine the overall error on the density. The density measurements for all three magnitude ranges agree with each other within errors for both absolute magnitude values individually.

5. Discussion

We have shown that we can successfully separate RC type stars from a background of disk type stars using a combination of kinematics and stellar surface gravities obtained from low resolution and signal to noise spectra. This procedure applied to an area of the sky in the direction of the trailing arm of the Sgr provides results that agree with previous measurements published on the stream. In particular, the distances and kinematics of our sample match other populations of stars both qualitatively and quantitatively. We also make the first measurement of the density of RC stars at a point along the tidal streams and find a value of $\rho = 2.7 \pm 0.5$ RC stars kpc⁻³. This

Table 5: RC Densities

Bright Limit	Abs. Magnitude	Volume (kpc ³)	Densities (stars kpc ⁻³)	
			Scaled	Integral
$g_{\circ} > 16.5$	$g_{abs} = 0.7$	24.0	1.52 ± 0.29	1.53 ± 0.28
	$g_{abs} = 1.0$	15.8	2.29 ± 0.43	2.31 ± 0.43
$g_{\circ} > 17.4$	$g_{abs} = 0.7$	21.0	1.60 ± 0.31	1.59 ± 0.30
	$g_{abs} = 1.0$	13.9	2.42 ± 0.46	2.40 ± 0.46
$g_{\circ} > 17.85$	$g_{abs} = 0.7$	17.4	1.76 ± 0.33	1.81 ± 0.33
	$g_{abs} = 1.0$	11.5	2.66 ± 0.49	2.74 ± 0.50

density was found using the faintest magnitude limit, star counts determined from the integral of the Gaussian fits to the kinematic peaks and using an absolute magnitude of $M_g = 1.0$. We consider these criteria the best for several reasons. First, our RC candidate stars seem to be concentrated at the faintest magnitudes. Second, the fit to the kinematic peak eliminates problems with choosing an arbitrary velocity range for the stream. Finally, the derived absolute magnitude matches the Sgr RC properties and is in good agreement with previously published distances to the stream.

Since the RC population of stars in the Sgr system seems to be a sizeable sample, one should be able to probe differences in densities of stars stripped from the galaxy proper. We note that while BHB stars are much easier to isolate photometrically, the RC stars we have observed are much more dynamically cold according to Figure 13. Identifying RC stream members should therefore be easier because of their large number and cold kinematics when compared to the BHB stream stars, which are harder to distinguish from the general halo field.

In a paper in preparation, we will present the density measurement of RC stars in another area of the streams and make a comparison with the results found here. This comparison coupled with previous (and future) investigations will give an idea of how and when the young population stars were stripped from the Sgr proper during previous orbits. Gradients along the stream of PopI stars has been suggested in Bellazzini et al. (2006) but more measurements of several different populations is needed for a complete accounting of the interaction history. Detailed measurements of the distribution of stars along the tidal streams will also make it possible to compute the total mass

in the stream and will provide information on the original distribution of these stars in the Sgr. This is crucial for determining the IMF of the original galaxy. Furthermore, determining the densities and locations of different populations of stars in the tidal streams will provide constraints on the internal dynamics of the original Sgr. This information is needed for better and more accurate models of the Sgr interacting with our Galaxy.

The Sgr orbiting in and around the potential of our Galaxy offers a unique opportunity to study an interacting galactic system. The RC population can be used as an effective probe to help constrain both the shape of the dark matter halo and the initial distribution of stars in the Sgr galaxy. We have shown that this population of stars can be extracted from the significant background and yield results which are consistent with other populations of stars. Several different populations of stars with different ages are needed to fully characterize the interaction of the Sgr with our Galaxy and the RC is a justifiable and observable group to use as a young/intermediate component.

We would like to acknowledge the NOAO for granting time and providing funding to make the necessary observations for this research. Funding was also provided by the Texas Space Grant Consortium and the Sigma Xi Grants In Aid of Research Program. This work was also supported by the National Natural Science Foundation of China under grants 11150110135, 11073026, and 11178013 and the Chinese Academy of Sciences under grant KJCX2-YW-T22 and the fellowship for young international scientists.

Funding for the Sloan Digital Sky Survey (SDSS) and SDSS-II has been provided by the Alfred P. Sloan Foundation, the Participating Insti-

tutions, the National Science Foundation, the U.S. Department of Energy, the National Aeronautics and Space Administration, the Japanese Monbukagakusho, and the Max Planck Society, and the Higher Education Funding Council for England. The SDSS Web site is <http://www.sdss.org/>.

The SDSS is managed by the Astrophysical Research Consortium (ARC) for the Participating Institutions. The Participating Institutions are the American Museum of Natural History, Astrophysical Institute Potsdam, University of Basel, University of Cambridge, Case Western Reserve University, The University of Chicago, Drexel University, Fermilab, the Institute for Advanced Study, the Japan Participation Group, The Johns Hopkins University, the Joint Institute for Nuclear Astrophysics, the Kavli Institute for Particle Astrophysics and Cosmology, the Korean Scientist Group, the Chinese Academy of Sciences (LAMOST), Los Alamos National Laboratory, the Max-Planck-Institute for Astronomy (MPIA), the Max-Planck-Institute for Astrophysics (MPA), New Mexico State University, Ohio State University, University of Pittsburgh, University of Portsmouth, Princeton University, the United States Naval Observatory, and the University of Washington.

Facilities: WIYN (Hydra).

REFERENCES

- Alonso, A., Arribas, S., & Martínez-Roger, C. 1999, *A&AS*, 140, 261
- Bellazzini, M., Ibata, R., Ferraro, F.R., & Testa, V. 2003, *A&A*, 405, 577
- Bellazzini, M., Newberg, H., Correnti, M., Ferraro, F., & Monaco, L. 2006, *A&A*, 457, L21
- Chou, M., et al. 2007, *ApJ*, 670, 346
- Correnti, M., Bellazzini, M., Ibata, R.A, Ferraro, F.R., & Varghese, A. 2010, *ApJ*, 721, 329
- Fellhauer, M., et al. 2006, *ApJ*, 651, 167
- Fukugita, M., Yasuda, N., Doi, M., Gunn, J.E., and York, D.G. 2011, *AJ*, 141, 47
- Gómez-Flechoso, M.A., Fux, R., & Martinet, L. 1999, *A&A*, 347, 77
- Helmi, A. & White, S.D.M. 2001, *MNRAS*, 323, 529
- Helmi, A. 2004a, *MNRAS*, 351, 643
- Helmi, A. 2004b, *ApJ*, 610, 97
- Ibata, R., Gilmore, G. & Irwin, M. 1994, *Nature*, 370, 194
- Ibata, R., Lewis, G.F., Irwin, M., Totten, E., & Quinn, T. 2001, *ApJ*, 551, 294
- Johnston, K.V., Law, D.R., & Majewski, S.R. 2005, *ApJ*, 619, 800
- Law, D., Johnston, K., & Majewski, S. 2005, *ApJ*, 619, 807
- Law, D. & Majewski, S. 2010, *ApJ*, 714, 229
- Layden, A. & Sarajedini, A. 2000, *AJ*, 119, 1760
- Lee, Y.S., et al. 2008, *AJ*, 136, 2022
- Majewski, S., Skrutskie, M., & Weinberg, M. 2003, *ApJ*, 599, 1082
- Majewski, S., et al. 2004, *AJ*, 128, 245
- Massey, P. & Jacoby, G.H. 1992, *ASP Conference Series*, 23, 240
- Mateo, M., Mirabal, N., Udalski, A. & Szymanski, M. 1996, *ApJ*, 458, L13
- McWilliam, A. 1990, *ApJS*, 74, 1075
- Newberg, H.J. et al. 2002, *ApJ*, 569, 245
- Percival, S.M. & Salaris, M. 2003, *MNRAS*, 343, 539
- Robin, A.C., Reylé, C., Derrière, S. & Picaud, S. 2003, *A&A*, 409, 523
- Ruhland, C., Bell, E.F., Rix, H.W., & Xue, X.X. 2011, *ApJ*, 731, 119
- Schönrich, R., Binney, J., & Dehnen, W. 2010, *MNRAS*, 403, 1829
- Shi, W.B., Chen, Y.Q., Carrell, K., & Zhao, G. 2012, *ApJ*, 751, 130
- Yanny, B., et al. 2009, *ApJ*, 700, 1282

This 2-column preprint was prepared with the AAS L^AT_EX macros v5.2.